Chapter 8.

DISCUSSION OF RESULTS: SUMMARY AND CONCLUSIONS.

8.1 Summary of Results.

The preceding three chapters contain a great deal of new experimental observations. Before attempting to account for these a summary of the main features to be explained will be useful.

a) In Chapter 5 we saw evidence that a field-evaporated metal ion follows a trajectory which is markedly different to that of the image-gas ions produced above it.

b) It was shown that the evaporation of a thick shell of material from the end of the field-ion specimen leads to a desorption image containing a great deal of fine structure. This structure has a common origin to the 'aiming errors' and apparently low detection efficiency from some specimen areas which are seen in the atom-probe.

c) The detail in the desorption images consists of dark and bright line systems, the origins of which are not immediately obvious from the normal field-ion image. The centres of major planes frequently appear dark, especially at very high evaporation rates, and are frequently surrounded by ring systems.

d) Some small changes in the details of the patterns are observed when the evaporation rate is changed from 1 plane/second to 10^8 planes/second.

e) Provided that the general state of the surface is unchanged, imtroducing an imaging-gas produces only minor changes in the desorption image.

f) There is a general similarity between the desorption images of the F.C.C. transition metals; the desorption image from copper is slightly modified. The transition metals show a pattern of bright lines radiating from {111} and {200} planes: in the case of iridium the desorption patterns obtained from Ir^{2+} and Ir^{3+} alone are very similar.

g) The non-transition series F.C.C. metal aluminium has a desorption image unlike any other metal so far studied. The amount of detail in this pattern is increased dramatically by lowering the temperature from 78°K to 20°K. Lowering the temperature of tungsten from 78°K to 20°K sharpens the detail in the image quite considerably, but unlike aluminium does not induce great changes in the character of the image.

h) Grain boundaries are clearly visible in the desorption images as bright or dark lines, or both, even when the change in the gross curvature of the surface across the boundary is expected to be slight. Ring systems cut by a grain boundary exist independently in the desorption images of the adjacent grains.

8.2 Scale of Details in Desorption Images.

The physical scale of the features in the desorption images can be estimated quite simply by using the inherent atomic resolution of the field-ion microscope to establish a distance scale which can be transferred to the desorption image from the same surface. The distance scale can be taken directly from the known interatomic spacing of well-resolved atoms, or indirectly, by counting the number of net rings between two poles of known angular spacing.

When this was done for a 20°K tungsten specimen, which had been desorbed both by nanosecond pulses and continuous evaporation, the following dimensions were obtained:-

Tip radius ~ 510 Å (51 nm.)

Diameter of first dark 110 ring ~ 90 Å (continuous evapn.)

Width of first dark 110 ring ~5 Å.

Diameter of dark central region of (110) 15-25 Å (continuous)

" " " " " " " 25-35 Å (nS-pulsed)

Width of 100 zone decoration ~9 Å.

Width of dark fringe around ⟨100⟩ zone decoration ~4 Å.

Width of dark lines radiating from (110) ~2,5 Å.

Total width of arms of dark 'propeller' radiating from {222} ~20 Å; these contain further structure on a scale of 4 Å which is dependent on evaporation rate and temperature.

Mean width of dark features crossing {211} planes, perpendicular to the close-packed rows, ~ 7 Å.

Similar measurements for the f.c.c. metals give the width of the characteristic bright zone-lines in the desorption images as 8-15 Å.

From the point of view of practical atom-probe work these results are fairly encouraging; the probe-hole of a normal atom-probe subtends a circle on the image corresponding to a diameter of approximately 20 Å referred to the specimen surface, while the dimensions given above show that the aiming errors in particular directions at particular regions of the specimen may have an uncertainty as little as 2,5 A. For the measurement of chapter 5, in which the diameter of {110} tungsten rings in the desorption image were compared with the rings in the helium image and found to be considerably smaller, the worst case found corresponds to a shift of only some 6 Å towards the centre of the (110) plane.

8.3 Tangential Energy and Aiming Errors.

It is instructive to calculate the tangential energy which, if it were the only factor involved in producing aiming errors, would be necessary to deflect ions over the apparent distances described above. Gomer(1961) calculated that a particle of mass m, charge ne, and transverse velocity v_t, would be displaced at the microscope screen by $2v_t x(2neV_o/m)^{-\frac{1}{2}}$, where x is the tip to screen distance, and V_o is the specimen potential. As the specimen magnification is x/r_t, where r_t is the specimen radius, the apparent shift on the specimen surface is

$$d = 2\beta r_t V_t (m/2 e V_o)^{\frac{1}{2}}$$

$$= 2\beta r_t \left(\frac{E_t}{n e V_o}\right)^{\frac{1}{2}}$$

where E_t is the ions transverse kinetic energy at the surface, and β is a small constant.

Substituting values for n=3, n=4 , with r_t=510 Å, V_o= 17 KV and β = 1 we obtain

d,A	E_t eV, n=3	E_t eV, n=4
3	0,5	0,67
6	1,8	2,45
12	7,2	9,6

It is seen that deflections due to thermal energies, of order kT = 0,01 eV, will be negligible at the low temperatures commonly used in field-ion microscopy. Any change in the desorption image as a function of temperature must be result of a change in the mechanism leading to a change in the transverse electronic energy of the ions.

8.4. The Origin of Aiming Errors.

8.4.1 Previous Explanations.

Before considering the desorption patterns in detail two previous attempts to explain aiming errors should be mentioned. First, Brenner and McKinney (1970) attempted to account for aiming errors by stating that the effect was due to parallax, as the image-gas ions are formed some distance from the surface:-

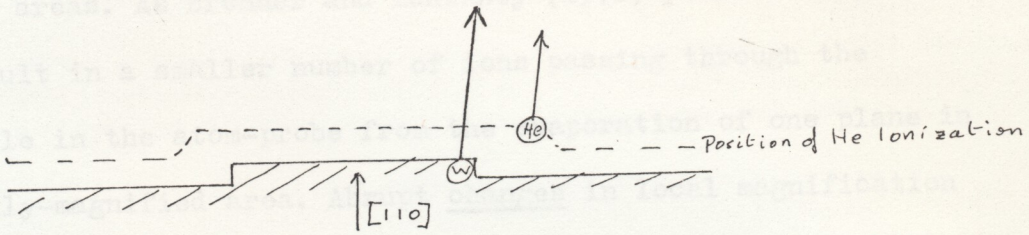

While this may be a contributory effect, if it is remembered that the metal ions will arrive at the critical distance for gas ionization with considerable kinetic energy, the considerable differences between the desorption images of, say, tungsten and iridium indicate that the true explanation is more complex than Brenner and McKinney suggested.

Second, in a very recent paper, Gillott (1975) has calculated the deflection of an ion's trajectory as a result of the changing electric field during pulsed evaporation. He found that there should be only a small deflection, in the opposite direction to that found by Brenner and McKinney, and he states that other processes must be involved. Since in the present work we have been largely concerned with DC-evaporation, pulse-effects will not be considered further.

We shall now consider the factors which are likely to influence the trajectory of metal ions and the formation of the desorption image. Three obvious factors are local magnification, surface diffusion before evaporation, and deflection after evaporation.

8.4.2 Local Magnification.

The magnification in the desorption image is given by $M = R/\beta r$, where R is the tip to screen distance, r the specimen radius, and β is a small constant. Specimen areas with a small local radius of curvature will be seen in the desorption image at a proportionately larger magnification than that of other specimen areas. As Brenner and McKinney (1970) pointed out, this will result in a smaller number of ions passing through the probe-hole in the atom-probe from the evaporation of one plane in the highly-magnified area. Abrupt changes in local magnification must tend to produce structure in the desorption image, and may account in part for the detail in the desorption image around, say, the $\{332\}$ planes in tungsten images. The magnification is not the only relevant factor in the production of structured desorption images, since altering the evaporation rate and temperature produces considerable changes in the desorption image of the tungsten 222 region, without any corresponding gross change in the local curvature as a justification for a drastic modification of the local magnification. Equally, there are no obvious reasons why the rhodium 110 zone-lines should be sufficiently demagnified to appear as bright lines in the desorption image, while the apparently similar endform of aluminium, imaged at 20°K in neon, should yield dark zone-lines.

It has been suggested (Muller and Tsong 1973) that the dark centres to planes in a desorption image may result from the increase in local magnification of the last few atoms left as a cluster at the centre of a plane. Again, this does not fit the experimental results; the local magnification should vary independently of the rate of evaporation, while it is observed that the dark centres to planes are generally larger at very high evaporation rates;

also, the centres of major planes are not always dark in the desorption image (viz. Gold{200} fig(6.7)).

8.4.3 Zone Decorations.

The field-evaporated endforms of many elements are commonly observed to be decorated along zone-lines by brightly-emitting atoms - the 'zone-decoration'. The appearance of the decoration is often a function of the evaporation temperature and rate (Muller 1964). As the zone-decoration atoms are resistant to field-evaporation and are sometimes seen to move from their original surface site, it is perhaps not unexpected that the field-desorption images are modified along the same zones as those which are decorated. For example, the ⟨110⟩ tungsten zone-decoration, which is an obvious feature of the field-ion image, is seen clearly in the desorption image as a bright area with a dark fringe; the breadth of the decoration is less in the desorption image than in the helium image. Also in tungsten, misplaced atoms are frequently seen on ⟨111⟩ zones, at 78°K; when tungsten is DC-evaporated at 78°K, the ⟨111⟩ zones are very bright in the resulting desorption image (fig(6.2)). The ⟨100⟩ zones in the {200} regions of f.c.c. metals (Pt, Au, Ir) are always decorated, and it is these zones which appear bright in the f.c.c. desorption image (the latter is true for rhodium, which does not show a zone decoration in helium or neon at 78°K). The origins of the zone decoration and the structure in the field-desorption image are therefore likely to be related.

Muller (1964) suggested that the zone-decoration atoms are atoms which are held in exposed sites on the surface by a gain of polarization energy in lieu of the lattice binding energy lost

as a result of the reduction in the number of near neighbours; that is, if $\frac{1}{2}\alpha_3 F_3^2 - \frac{1}{2}\alpha_4 F_4^2 \quad \frac{1}{2}(\alpha_3 - \alpha_4)F^2 \geqslant \Lambda/4$, the atom would move from a site with four neighbours to one with three ($\Lambda/4$ is the difference in binding energy between a kink-site and a metastable site, considering constant pairwise potentials between first nearest neighbours only. Tong and Gilman (1968) and Forbes (1970) found that at liquid helium temperatures the tungsten $\langle 100 \rangle$ zone decoration was formed from small clusters of 3,4, or 5 atoms in metastable sites, rather than single atoms, as stated by Muller (1964).

Muller attempted to calculate the polarizability by equating the electrostatic energy $\frac{1}{2}\varepsilon_0 F^2$ of the field inside the metal surface, assuming a small penetration distance λ, to the polarization energy of the surface atom. This equation, which he did not attempt to justify, resulted in in a value for the polarizability of 0,54 $Å^3$ for tungsten $\{110\}$, which is much less than the 4,6 $Å^3$ or 6,8 $Å^3$ obtained from evaporation rate measurements (Tsong and Muller 1970) or the 9,2 A^3 derived by Tsong and Walko (1972) from experiments on the random walk of adatoms in the presence of an electric field. Although Muller's (1964) calculations seem hard to justify (Ehrlich and Kirk 1967 conclude that polarization and field-penetration produce separate changes of opposite sign in the energy of a surface atom) the concept of a partial replacement of lattice binding energy by a polarization energy for an atom in a metastable site is reasonable.

8.4.4 Other Field Effects.

Several workers have noted the movement of surface atoms under the action of the electric field. For example, Bettler and

Charbonnier (1960) reported that the activation energy for surface self-diffusion was reduced by some ten percent at fields of 0,3-0,4 V/Å for a number of transition metals; Utsugi and Gomer (1962) found the activation energy for diffusion of Ba on tungsten became zero at 0,5-0,6 V/Å; in contrast, Bassett and Parsley (1963) found no change in the activation energy of diffusion for rhenium atoms adsorbed on tungsten.

Plummer and Rhodin (1968) observed that platinum ad-atoms diffused across the {222} and {112} planes of tungsten, and gold ad-atoms across the {110} and {200} planes, before evaporating. Boyes and Southon (1972) noted the rearrangement and diffusion of the last few gold atoms to evaporate from gold {111} planes, imaged at 20°K in neon. Plummer (1968) stated that the diffusion was the result of polarization forces, and deduced that the electric field could vary by 10% from the centre to the edge of a net plane.

8.4.5 Binding Energy in an Electric Field.

The binding energy of a surface atom, as a function of its position relative to a step in the surface, is of the form shown below (Schwoebel and Shipsey 1966).

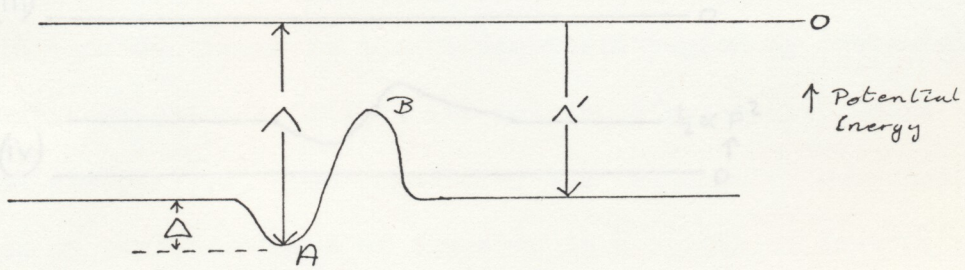

Here A represents the energy of the atom at a kink-site and B the energy as the atom is moved over the edge of the step. This diagram is obtained by summing the interatomic potentials (e.g.

Morse potentials) between the atom and its near neighbours. The binding energy Λ is given by Ehrlich and Kirk (1967) as 8,83 eV for tungsten, whereas the adatom binding energy Λ' is found experimentally to be 5,2 eV for {110} planes, 7,0 eV for {211}, and 6,0 eV for {111}, and from a Morse-potential calculation (Girifalco and Weizer 1959) to be 5,77 eV, 7,68 eV, and 7,93 eV respectively. The barrier Δ which prevents kink-site atoms from diffusing across the adjacent terrace is therefore of order 3,6-0,9eV, depending on the plane, in zero field. Graham and Ehrlich (1974) find the barrier to be 1,8 eV for tungsten {222} planes, from measurement of the diffusion rate as a function of temperature.

The potential diagram shown above will be modified in the presence of an electric field by the polarization energy of the atom, $\frac{1}{2}\alpha F^2$. This energy will be a function of the position of the atom; the polarizability will be greater when the atom is exposed to the field, and less when it is in a position screened by the conduction electrons; the field will be higher at the step, and will decrease on either side of it:-

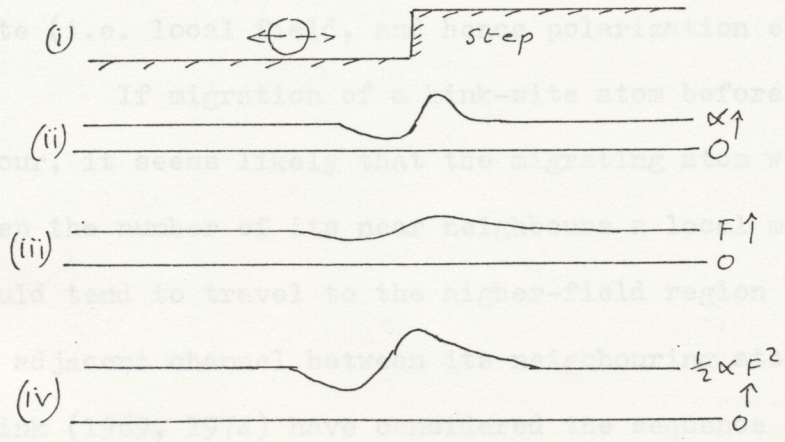

The polarization energy binds the atom to the surface, so the total potential energy of the atom = $-(|\Lambda| + \frac{1}{2}\alpha F^2)$ will become

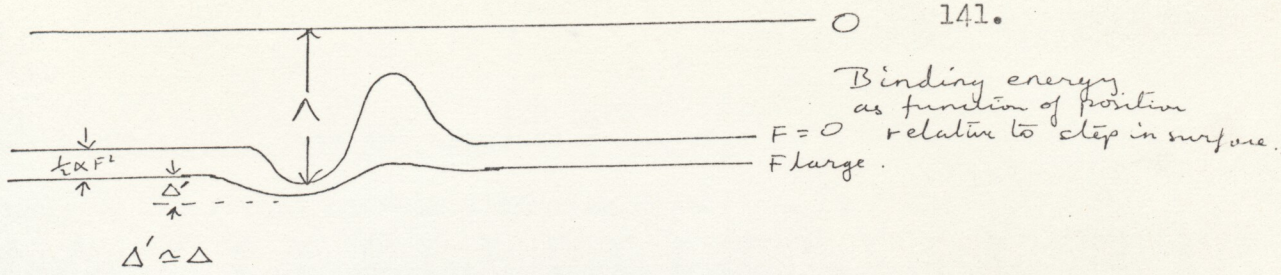

The barrier to diffusion across the terrace is little changed, but the barrier to diffusion up over the ledge is greatly reduced; the magnitude of this reduction is difficult to estimate, as neither the polarizability of the kink-site atom nor of an atom in an unstable site on top of a ledge are known; if the difference of the polarizabilities is say 3 $Å^3$ and the field is 10% higher on the ledge, a reduction of 3 eV at 5 V/Å would be easily possible. This raises the possibility that, prior to evaporation, a kink-site atom might move up onto the adjacent ledge, to a site more exposed to the field; ionization and field-evaporation would be likely to follow rapidly following this migration. This movement up onto the ledge would be an alternative to that shown by the zone-decoration atoms, which move across the terrace away from the step. In fact, movement across the terrace, or up over the step, could be a function of the plane under consideration, and of the evaporation rate (i.e. local field, and hence polarization energy).

If migration of a kink-site atom before evaporation did occur, it seems likely that the migrating atom would move so as to keep the number of its near neighbours a local maximum (that is, it would tend to travel to the higher-field region by moving along an adjacent channel between its neighbouring atoms). Moore and Spink (1969, 1974) have considered the sequence of evaporation of atoms on various planes of tungsten in a series of careful experiments, using 10 uS pulsed evaporation. They conclude that the order in which atoms evaporate depends on the availability of a suitable diffusion channel in the surface, adjacent to the evaporating atom's lattice site.

Fig. 8.1

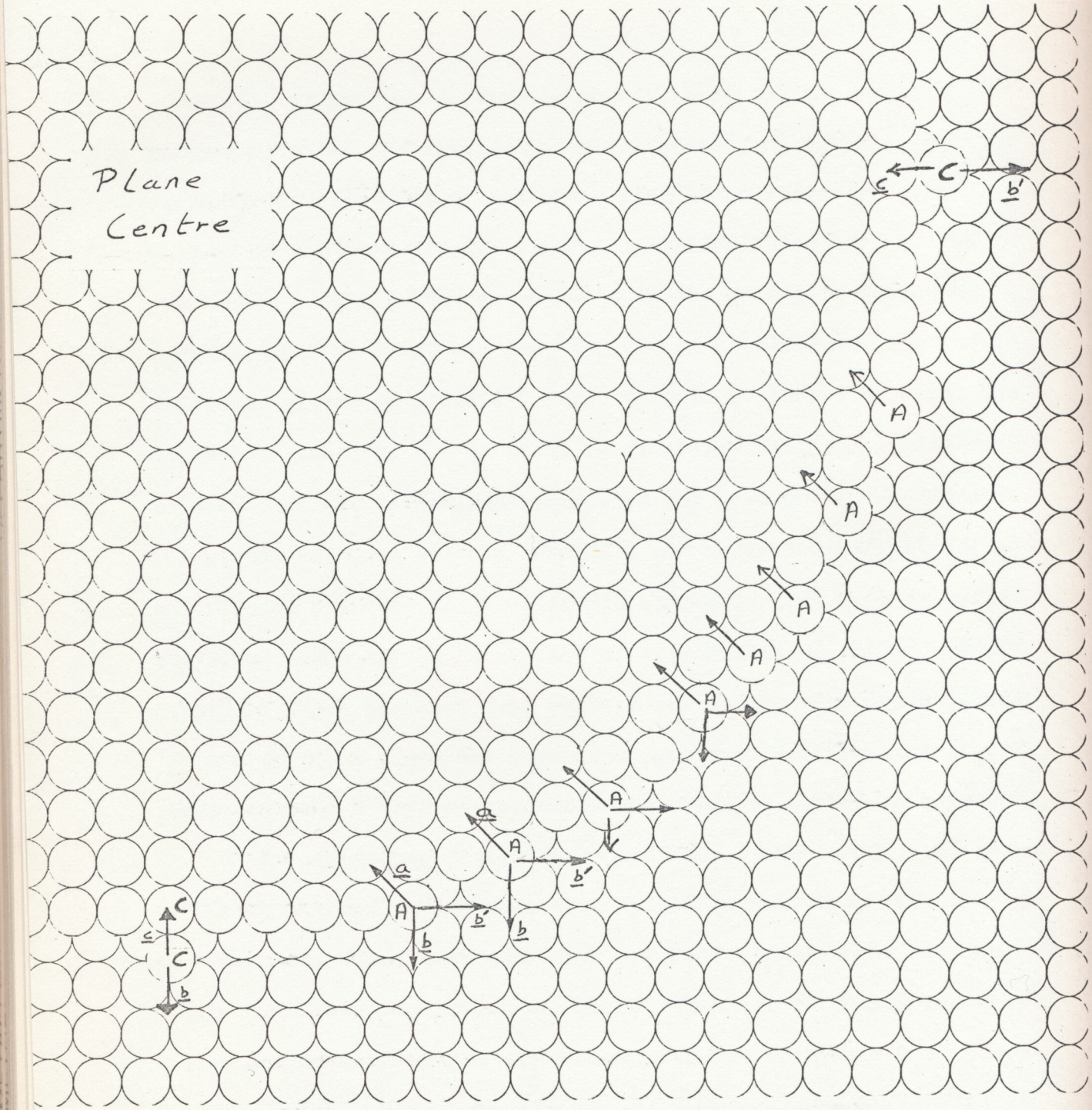

I am grateful to Mr. D.J. Garnett for producing the computer programme which was used to draw the atomic planes used in this Chapter.

8.5 Surface Diffusion and Desorption Images.

The likely surface diffusion directions, and the effect that such diffusion is likely to have on the desorption image, may be seen by inspection of a ball-model of the specimen surface. Photographs of typical surface structures for common crystal planes have been summarized by Nicholas (1965). We will briefly consider the possibilities for the more prominent planes of the f.c.c. and b.c.c. metals.

8.5.1 The F.C.C. Metals.

The environment of a kink-site atom on a circular {200} net plane may be seen from fig(8.1); it is seen that the kink-site atoms, labelled A, are all constrained by their neighbours to move in direction a if they move up over the step towards the centre of the plane, or in directions b, b' if they move away from the step across the terrace. As the plane evaporates, the last atom of the row, labelled C, is not able to be channelled in direction a; it must either travel up over the ledge in direction c, while in contact with only 1 near neighbour, or move away from the ledge in direction b. The appearance of single zone-decoration atoms at sites corresponding to C in the field-ion images of f.c.c. metals is thus accounted for; the atom C is unable to evaporate in the same manner as its neighbours, and therefore migrates onto the terrace, where it is retained until its local field becomes high enough to allow evaporation in some other manner.

For the {111} planes, (fig(8.2)), the optimum diffusion directions are as shown. The kink-site atom A can move up over the step in directions a_1, a_2, or a_3 and away from the step across

Fig. 8.2

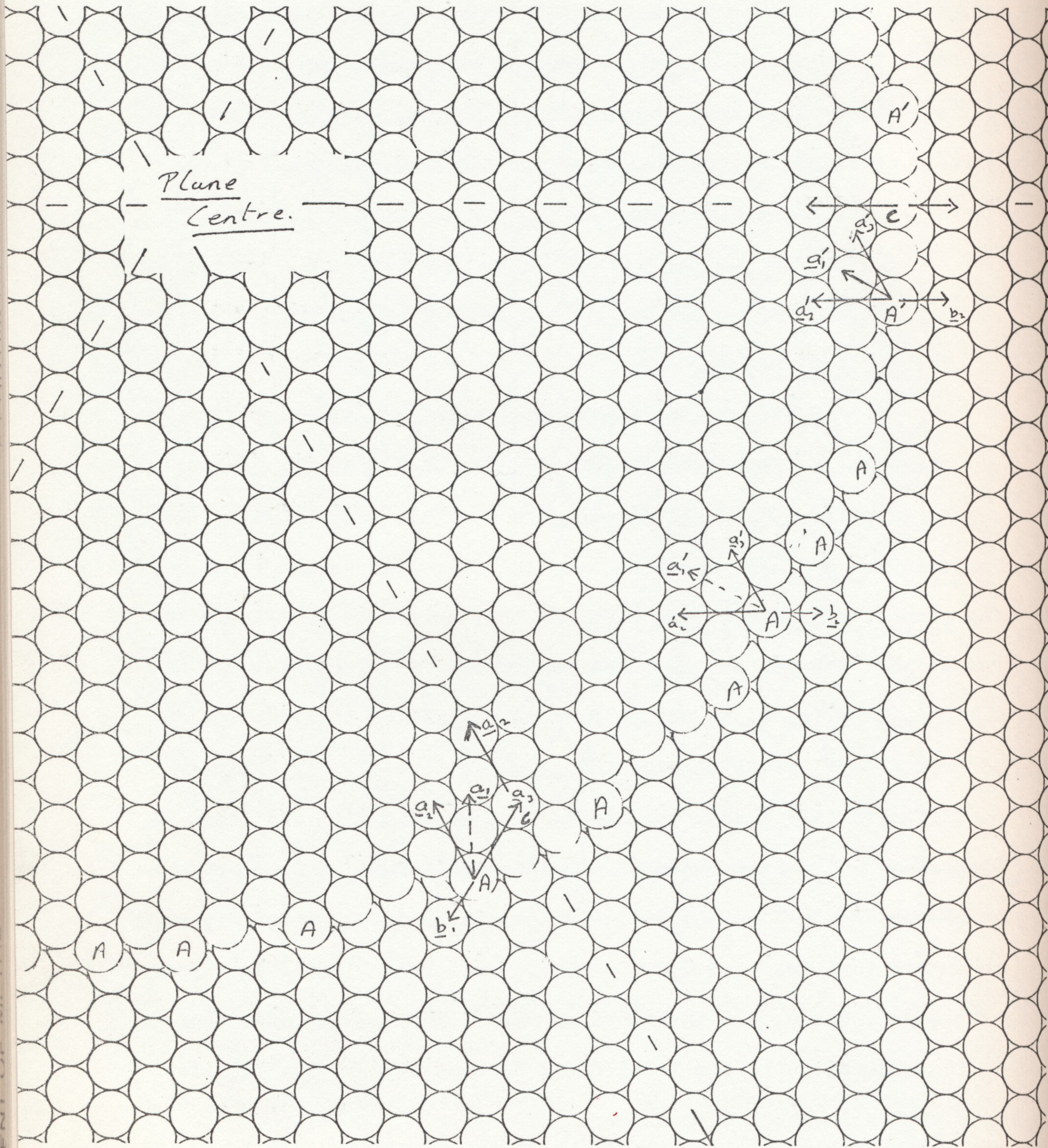

the terrace in direction $\underline{b}_1$, $\underline{b}_2$. In direction a_1 the atom has one nearest neighbour and two second nearest neighbours, while in directions $\underline{a}_2$, $\underline{a}_3$ it retains two first-nearest neighbours and one more distant neighbour. The last atoms of the rows, C and C', are still able to move up over the ledge in directions $\underline{a}_2$ or $\underline{a}_3$, without any prior movement along the ledge, as well as moving away from the step along $\underline{b}_1$ or $\underline{b}_2$; this fits the experimental observation that f.c.c. {111} planes do not generally have zone-decorations.

Further analysis of higher-index planes ({220} {311} etc.) has been carried out, but will not be described in detail here; as the plane becomes rougher it becomes progressively more difficult to determine the likely diffusion directions; however, as the most prominent planes on an f.c.c. specimen are the {111} and the {200}, we shall now consider the likely effect of the above conclusions on the desorption image.

It is plausible to assume that if a kink-site atom is channelled in a particular direction up over the adjacent step under the influence of strong polarization forces, it will arrive in a region of enhanced field with some considerable kinetic energy. If ionization and subsequent evaporation is virtually instantaneous, this kinetic energy may be retained by the ion, and will tend to propel the ion further along its initial channelling direction. Since, as we have seen, all kink-site atoms of a net plane will have well-defined crystallographic channelling-directions, the resulting bulk movement of ions will have a considerable effect on the desorption image. For the {111} and {200} planes discussed above, the situation, and expected desorption images, are sketched in fig(8.3). Overlap in the trajectories of ions from adjacent sectors with different surface channelling directions

(a)

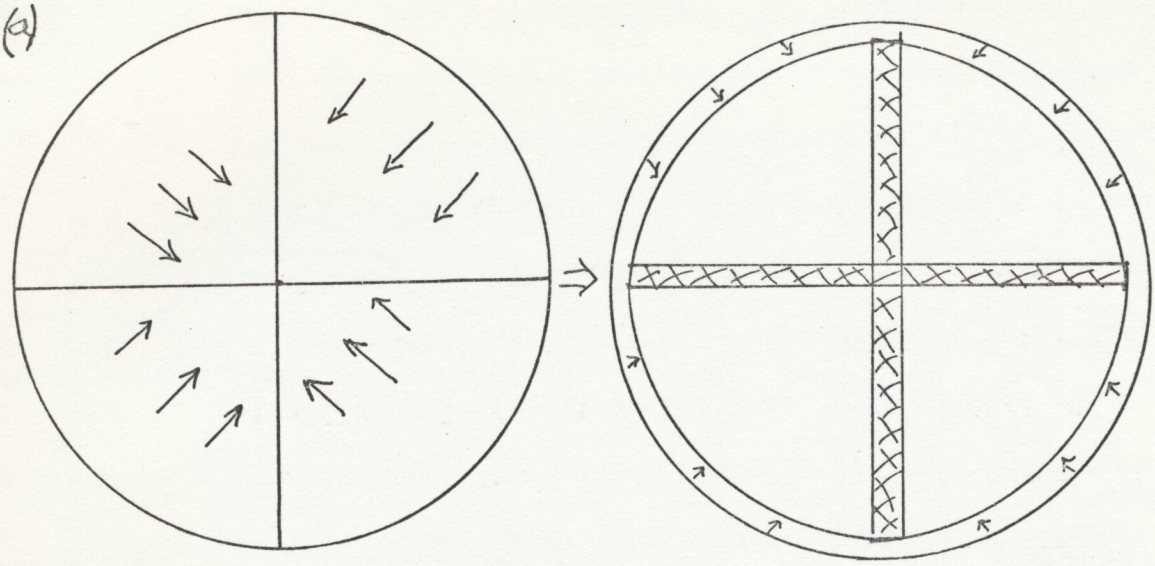

(b)

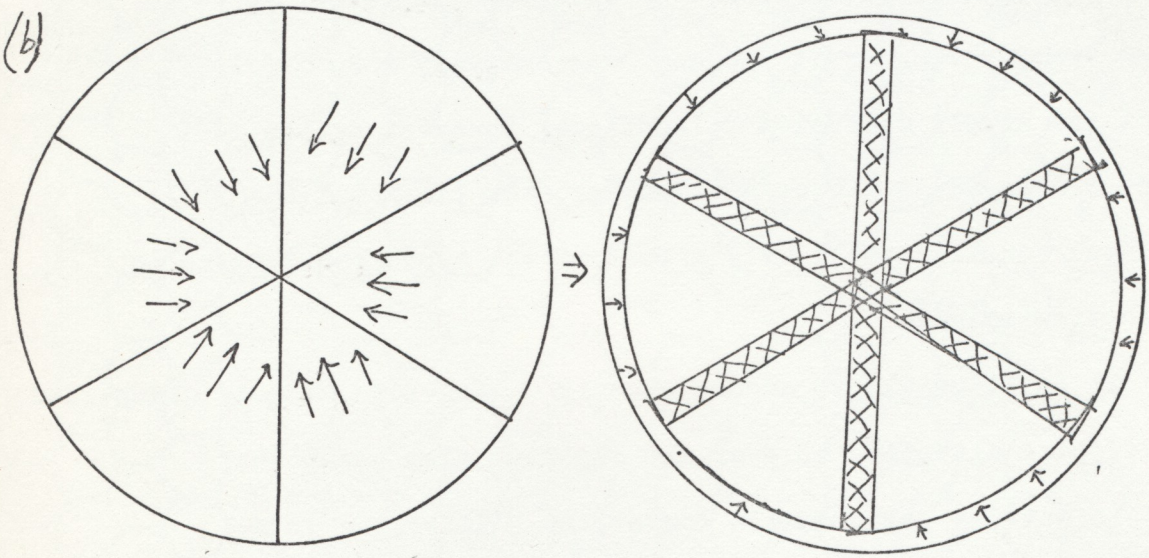

(c)

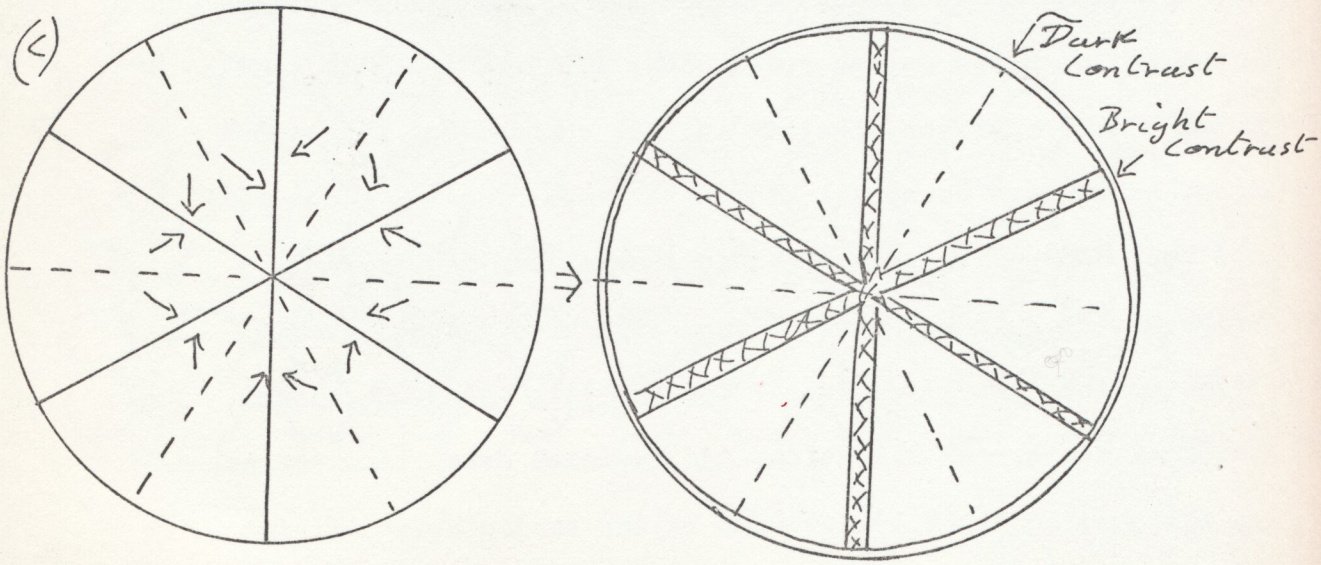

will lead to a doubling of the number of ions/unit area in some areas of the desorption image. Two types of {111} images are shown, one for the directions $\underline{a}_1$ of fig(8.2) and the other for directions $\underline{a}_2$, $\underline{a}_3$. The latter lead to the appearance of dark lines intermediate between the bright lines, in remarkable agreement with the iridium desorption pattern, fig(6.15).

The circumstantial evidence that channelled diffusion up over the ledge leads to the appearance of the typical f.c.c. desorption pattern is good. To summarize it,

a) This model predicts the appearance of pseudohexagonal symmetry for the desorption images of {111} planes.

b) The bright-line contrast is predicted to be roughly twice as intense as the local background; as nearly as may be judged by counting the number of scintillations/unit area in the desorption image (e.g. fig(7.4)) this is correct.

c) The failure of the ⟨100⟩ zone decoration atoms to evaporate at the same field as their neighbours, but rather to move into a metastable site, is explained.

d) If there are bulk movements of ions in particular crystallographic directions, there will be particularly dark contrast in the desorption image when the directions in two adjacent sectors are opposite;

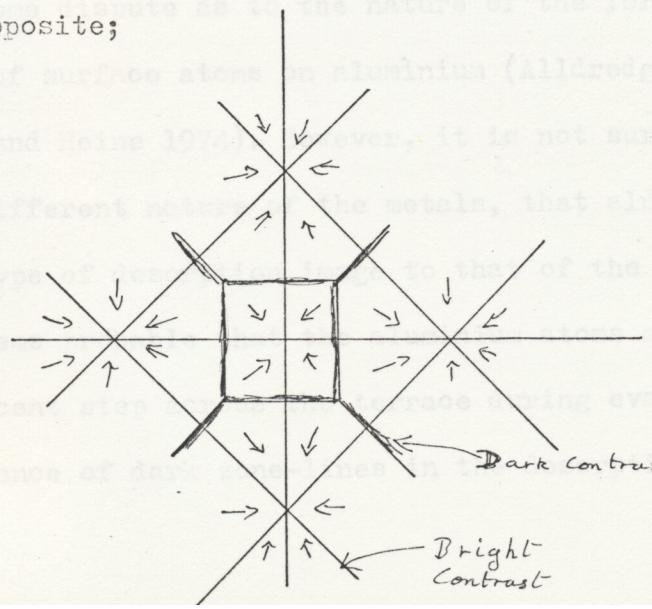

This dark contrast is exactly what is seen in the desorption image (e.g. gold fig(6.7)); the dark contrast in these areas will also be partly due to the higher local magnification, as the dark lines follow the highest-field regions of the f.c.c. specimens.

This simple model accounts fairly succesfully for the appearance of the desorption images from the refractory f.c.c. metals. Does it also account for the different appearance of the desorption images from copper and aluminium? The prime assumption that was made above is that the diffusing atoms can be treated as hard spheres in contact with one another. This is a good approximation for the transition metals, in which the attraction between the ion cores and the conduction electrons is balanced by the steeply-rising repulsive potential due to the overlap of the outermost electrons of the cores. Copper is somewhat different to the other f.c.c. metals in that it has a full d-band and one s-electron; the interatomic potential may be expected to be modified. In the case of aluminium, we have an sp metal in which the ion cores may be considered to be completely separated by the conduction-electron gas; this gives aluminium different mechanical properties to those of the transition metals, and in particular the interatomic potential does not rise so steeply as the ion-cores approach one another. There still seems to be some dispute as to the nature of the forces on and displacement of surface atoms on aluminium (Alldredge and Kleinman 1974, Finnis and Heine 1974). However, it is not surprising, in view of the different nature of the metals, that aluminium produces a different type of desorption image to that of the refractory f.c.c. metals. It seems probable that the aluminium atoms migrate away from the adjacent step across the terrace during evaporation, leading to the appearance of dark zone-lines in the desorption image. The

Fig. 8.4

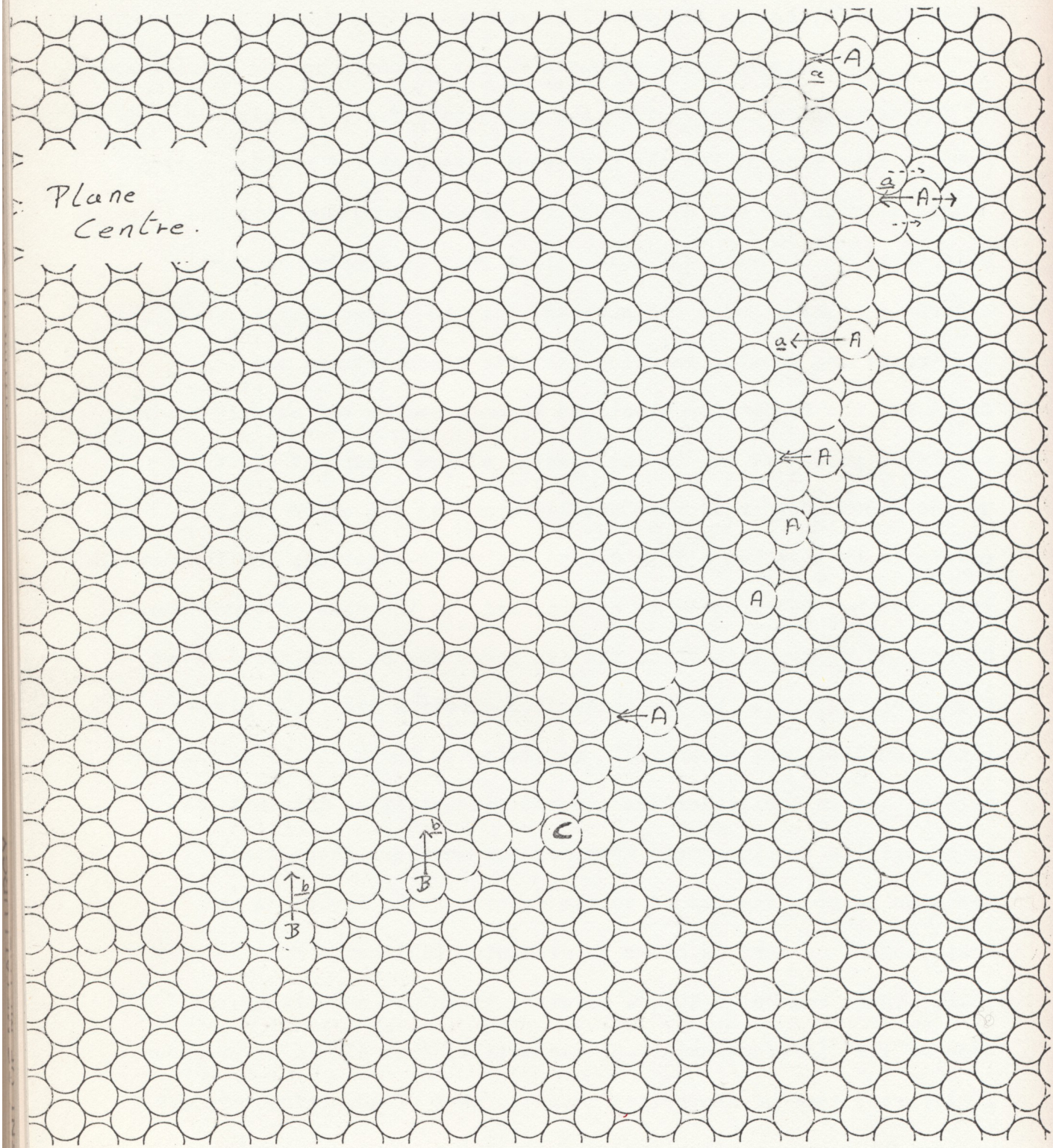

precise nature of this migration, and in particular the way it changes as a function of temperature (and hence field, or polarization energy) are not understood at present. The unexpectedly high evaporation field of aluminium (Brandon (1964) predicted only 1,8 V/A) may be due to the difference in evaporation behaviour.

8.5.2 The B.C.C. Metals.

We may apply the same type of hard-sphere analysis to the less closely-packed B.C.C. structure. For the {110} plane (fig(8.4)) the kink-site atoms A, B can migrate up over the step towards the plane centre in directions a, b; atom A can also relax in the reverse direction to a into the adjacent metastable zone-decoration site on the terrace, as suggested by Muller (1964). When the normal kink-site atoms A, B have evaporated, the atom C is left at the end of one of the close-packed rows and is unable to migrate up over the step without prior diffusion on the terrace. It is commonly observed (e.g. Taylor 1970) that at liquid-nitrogen temperature the atoms at the ends of the close-packed rows are resistant to evaporation and frequently migrate short distances before evaporation. The positions of these evaporation-resistant atoms coincide with the bright-line contrast seen in the 78°K tungsten continuous-evaporation desorption images(fig(6.2)). This contrast is very marked at high temperatures, but not under nanosecond-pulsed evaporation at 78°K or continuous or pulsed evaporation at 20°K. Consideration of the possible overlap between the trajectories of ions from different specimen areas predicts the same bright contrast along these ⟨111⟩ zone lines as on the f.c.c. ⟨100⟩ zone-lines. However, the disappearance of the bright contrast

at low temperatures and high evaporation-rates suggests that the mechanism is more complicated than for the f.c.c. metals. A measurement of the aiming-error in this region as a function of temperature and evaporation rate would shed light on this problem. As we are here concerned with the interpretation of the vacuum desorption image, the method of Chapter 5, which relies on the prior field-ion imaging of the surface, is not appropriate, as the presence of helium is known to affect the evaporation behaviour, to an extent which is dependent on the field and temperature (Chapter 7). The determination of the exact way in which the evaporation of tungsten occurs is not trivial,for this reason.

If the ⟨110⟩zone-decoration atoms move away from the original plane edge to metastable sites, before finally evaporating, it is not surprising that the zone-decoration appears distinctly on the desorption image. It is not quite so obvious why the zone-decoration is narrow in the desorption image, while in the helium image it is seen as a broad band of bright atoms (although the magnification of individual atoms in the zone decoration is large, especially at high temperatures, the extent of the decoration across the surface should not be subject to such a large change in local magnification). It is possible that the introduction of helium into the system after vacuum desorption leads to a broadening of the zone decoration, as a result of the change in atomic potential due to the polarizing effect of field-adsorbed helium: vacuum evaporation, followed by the admission of helium at a very low temperature ($< 20^{\circ}K$) to minimize thermal excitations, and at as low a field as possible, to minimize polarization energy, might perhaps reveal a narrow zone-decoration corresponding to the vacuum-evaporation zone-decoration.

On the b.c.c. {200} planes (fig(8.5)), migration of the

Fig. 8.5

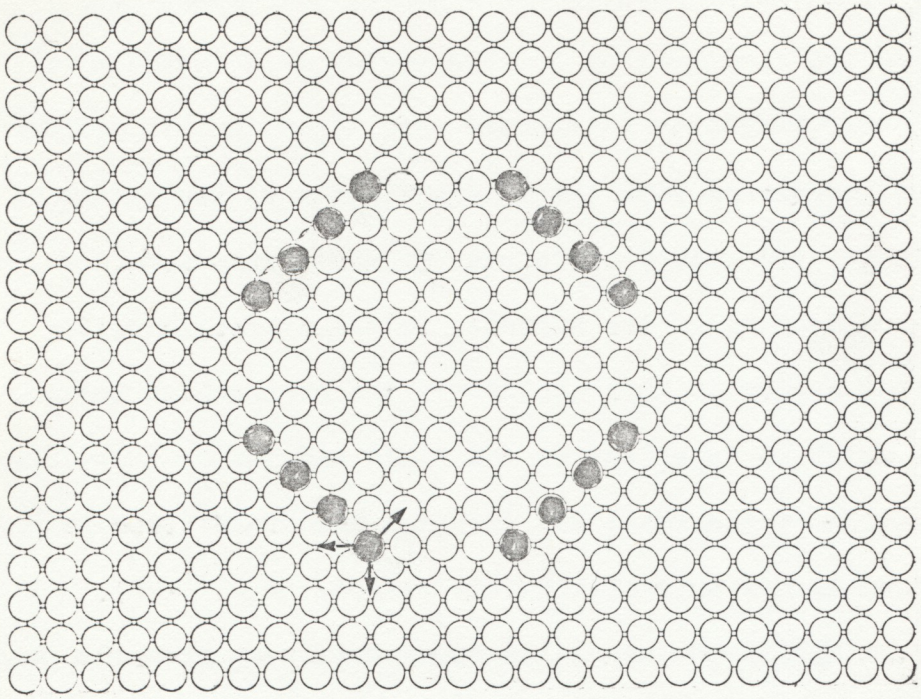

Fig. 8.6

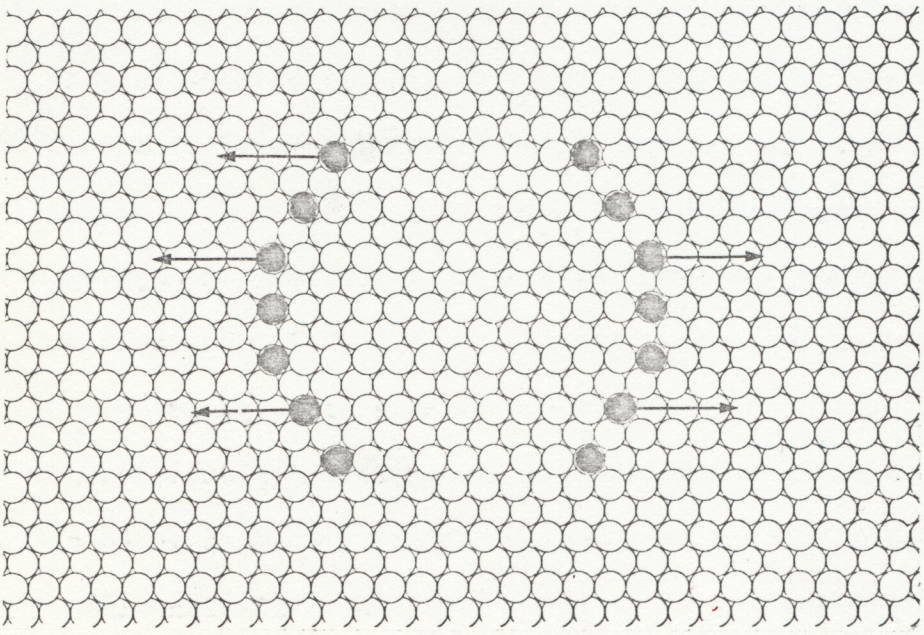

kink-site atoms towards the plane centre involves one nearest neighbour and two second-nearest neighbours; diffusion across the terrace in the ⟨001⟩ directions is easy, and the diffusing atom retains contact with two near neighbours. The ragged appearance of the tungsten {200} regions suggest that atoms migrate in this latter manner, and are not evaporated immediately, but rather settle in new sites further from the plane centre. The ragged nature of this region may be responsible for the diffuse appearance of this region in the desorption image.

The {211} planes of b.c.c. metals consist of close-packed rows some distance apart (fig(8.6)). Ehrlich and Kirk (1967) found that the activation energy for diffusion along the rows is only 0,57 eV for tungsten ad-atoms. The last few atoms to be evaporated from tungsten {211} planes are commonly seen in the helium image to be spread out along the surface channels; somewhat similar behaviour is seen in molybdenum also. It seems reasonable to conclude that tungsten atoms diffuse down the channels for some distance before evaporating; the result of this in the desorption image is the dark linear centre to the plane perpendicular to the close-packed directions.

The evaporation behaviour of tungsten {222} and adjacent planes has been studied by Moore and Spink (1974), who found that surface diffusion before evaporation was likely. As has been pointed out above, the desorption image of this region is a function of the evaporation field. It seems likely that changes in polarizability and hence of polarization energy for different diffusion directions occur as a function of field, which is very high in this region, and this causes a change in the diffusion directions which are favourable at different fields. The central region of this plane is dark in

low-temperature desorption images: however, above 78°K at slow evaporation rates some structure becomes visible at the centre of the plane. It is possible that evaporation may take place almost directly from lattice sites under these conditions; further experiments to see if the {111} lattice can be resolved under these conditions would be of interest, as there seems to be no other case, in the materials which have been studied to date, which is likely to yield the resolution of a net plane of the lattice, since other plane centres are either dark, implying some gross deflection of the ions' trajectories, or contain structure due to the f.c.c. desorption image, which is only indirectly due to the lattice.

It is seen that the hard-sphere surface diffusion model is reasonably successful in the case of tungsten. However, the behaviour of tungsten is more complicated than that of the f.c.c. transition metals. The very different helium and desorption images of tantalum and molybdenum suggest that the model may need some modification, to take into account directionality of bonding and differences in polarization energy, which seem to play some part in determining the different endforms of the refractory b.c.c. metals (Nakamura and Kuroda 1979).

8.5.3 Grain Boundaries.

No detailed analysis of the appearance of grain-boundaries will be given here. However, it should be noted that the arguments which have been discussed above may be relevant to the desorption images of grain-boundaries. Suppose that there is a well-defined surface channelling direction in a specimen area adjacent to a

grain-boundary, so that ions are deflected towards the boundary. The last few atoms to evaporate from this side of the boundary will do so from a misoriented lattice. If there are not easy channelling directions presented by the lattice on the other side of the boundary the last few atoms may be retained, and evaporate at a somewhat higher field with a different trajectory, probably leading to a bright line in the desorption image at the boundary. There will be an adjacent dark line if the ions from the other side of the boundary have been channelled away from it by their local surface geometry.

8.5.4 Plane Centres.

The dark centres to major planes are very pronounced at high evaporation-rates (and hence high fields). The possible explanations for this are:-

a) At some fields the balance between the binding energy of the net plane and the polarization energy of its constituent atoms may be such that the plane breaks up, with atoms diffusing away before evaporation. As mentioned above, this type of behaviour has been seen at normal imaging fields and low temperatures for gold {111} planes (Boyes and Southon 1972). It is also known that the interatomic binding energy may be reduced for small clusters of atoms (Bassett 1970).

b) If the last few atoms on a plane evaporate simultaneously, there will be strong coulomb repulsions between them (even after allowing for their image potentials in the metal surface). This repulsion will lead to deflection of the ions away from the centre

of the plane in the desorption image. For this process to occur the ions would have to evaporate within a very short time of one another, as they are rapidly removed by the field. This time is estimated as of the order of 10^{-15} seconds; unless the removal of one ion is directly responsible for the ionization of the others, this mechanism seems to be less likely than the mechanism given in (a) above.

8.5.5 Ring Structures.

One of the most puzzling features of the desorption images is the appearance of dark rings around major poles; as explained above, these are obtained even after the evaporation of hundreds of net planes to form the desorption image. Since they exist independently in two crystals separated by a grain boundary, they must be a property of the lattice. They imply that there is a periodic fluctuation in the magnitude, or direction, of the aiming error near the pole. The breadth of the dark rings, or polygons, for tungsten {110} at 20°K was given above as some 5 A, corresponding to a change in tangential energy of at least 1,5 eV; this implies that the rings are due to an electronic or field effect, rather than, say, a lattice effect, as phonon energies are generally much smaller than this.

A possible explanation may be the following. Consider a circle radius R drawn round a well-developed hkl pole on the specimen surface. Let the mean field inside this region be F_o. From Gauss' Theorem, the charge inside the circle $\simeq \pi R^2 F_o \varepsilon_o$. Suppose that the mean radius of curvature of the specimen is S; then if the spacing of the {hkl} planes is d, the radius of the n^{th}

{hkl} net plane will be given by

$$r_n^2 = (2S - (n + \delta)d)((n + \delta)d) \quad 2S(n + \delta)d$$

where $0 \leqslant \delta < 1$ gives the diameter of the innermost (n = 0) plane.

We know that the field at the edge of each net plane is the same evaporation field F_e; the field decreases away from the edge of each plane:-

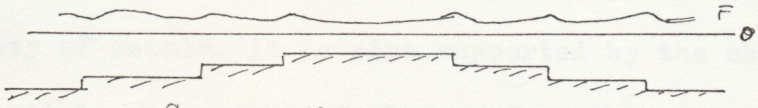

Suppose that to a first approximation the field decreases linearly from the edge of each net plane in towards its centre:-

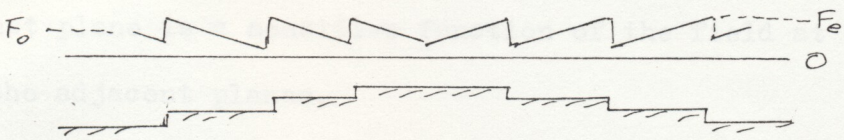

or $F(r) = F_e - k(r_n - r)$ where $r_n > r > r_{n-1}$.

The total charge inside the n^{th} ring will therefore be given by $Q = \int \varepsilon_o F \, dS = 2\pi\varepsilon_o \sum_{n=0}^{n} \int_{r_{n-1}}^{r_n} (F_e - k(r_n - r)r \, dr$

and, after adding any charge for an incomplete $n+1^{th}$ ring, this must equal the value obtained from the 'average field' obtained above. It seems clear that if $k \neq 0$, then k cannot be a constant, since, for example, the total perimeter of the net plane edges inside our radius R, on which a large part of the charge resides, and on which the field is fixed at F_e, fluctuates periodically as the parameter δ changes between 0 and 1;

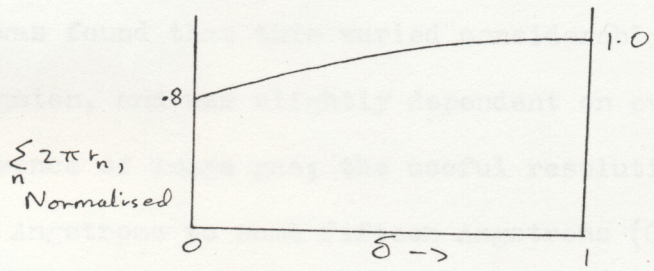

Now if k varies periodically, as the central net plane evaporates, then it seems likely that the aiming error, which must depend on the spatial variation of the field at the edges of the net planes, will also fluctuate periodically. Until a full three-dimensional

calculation of the field and its variation with net plane diameter becomes available, this theory must be considered speculative. The fact that the diameters of the desorption-image rings obey the same n relationship as the field-ion images of the net-planes lends some support to this simple theory, as does the fact that the rings are seen on more-or-less any well-developed plane of a wide variety of metals. It is also supported by the observation of sequential evaporation of planes, from the central plane outwards (Chapter 7) which implies that the local field at the edge of a net plane is a sensitive function of the field at the edges of the adjacent planes.

8.6 Summary.

In this chapter we have seen a summary of the essential features of the desorption images described in Chapters 5-7. The dimensions of particular features were estimated, so that an idea of the useful spatial resolution of an atom-probe could be obtained. It was found that this varied considerably from plane to plane in tungsten, and was slightly dependent on evaporation rate and the presence of image gas; the useful resolution lies between one or two Angstroms to some fifteen Angstroms (0,2-1,5 nm.). The tangential energy required to deflect ions of various charges over comparable distances was calculated. An account followed of previously-known interactions of the electric field with the surface atoms, to produce atoms shifted from normal latttice sites and zone-decorations.

This introduced a brief discussion of the way in which the binding-energy of a kink-site atom would be affected by the field; this suggested that field-evaporation might occur, not directly from the kink-sites, but rather via thermal activation or tunnelling through a reduced barrier along a surface channel, bounded by neighbouring atoms. This very simple model predicts the desorption patterns from the refractory f.c.c. {111} and {200} planes with some success; it was suggested that aluminium behaves differently as a result of its very different type of interatomic potential. The model also had some limited succes with the b.c.c. (tungsten) desorption image. A brief discussion was given of the origin of dark centres to planes in the desorption image, and a tentative explanation for the frequent observation of ring-structures surrounding such planes was advanced.

8.7 Suggestions for Future Work.

The experimental evidence on the field-evaporation process which has been described in this dissertation, both the work on the energy of field-evaporated ions described in Chapter 4, and the work on field-desorption summarized in this chapter, has perhaps raised as many questions as have been answered. The use of energy-analysis as a tool for investigating field-evaporation has been established: the results obtained so far suggest thatfurther investigation will be useful. The work presented here on field-desorption has served to show that the field-evaporation process is sensitive to the local environment of the evaporating atom; the previous treatment of

field-evaporation as the removal of an ad-atom from an infinite plane is no longer acceptable as a description of the evaporation-behaviour of kink-site atoms on a crystal with a sharply-curved surface. The hypothesis outlined above, the channelling of atoms during evaporation into high-field sites by the interaction of electrostatic and interatomic forces, may perhaps be fairly compared with the role of dislocations in determining the deformation of metals; the channelling process apparently offers an easier path to field evaporation, as the dislocation provides as easier indirect way of deforming a metal. It is to be hoped that it will become possible to calculate the polarizabilities of surface atoms and the trajectories of the resultant ions , so that the validity of the conclusions reached above may be tested.

As to the use of the atom-probe as an instrument for chemical analysis, it is now clear that, in general , it is not possible to chemically analyse a metal atom-by-atom at present; unless and until it becomes possible to deconvolute the effects of the evaporation process from the desorption image this must be considered impractical.However, although the desorption images from single crystals of pure elements have been shown to be complex, the ragged nature of the specimen surface of many alloys may actually prove to be advantageous, in limiting the possibility of surface diffusion over long distances prior to evaporation. Equally, the little work which has been done so far in the presence of imaging gas suggests that aiming errors may be less in some instances than in vacuum; there is no reason at present to believe that they are worse. Further work to establish the accuracy of these conclusions is essential.

The desorption atom-probe, of which a simple version was

described in Chapter 7, has been clearly established as a useful instrument, both for the investigation of field-evaporation, and for use as a metallurgical tool. Since imaging-gas is not an essential requirement for field-desorption microscopy, it seems possible that this instrument could be used to investigate materials (e.g. magnesium alloys, brasses) and processes (catalytic reactions) which are adversely affected by the high electric field necessary for field-ion imaging. The only requirement now is that it should be possible to field-desorb the specimen for analysis, thus allowing the application of the field-ion technique to a wider range of problems than ever before.